

Received: 2015.10.15
Accepted: 2015.12.01
Published: 2016.07.01

Pulsatile Support Mode of BJUT-II Ventricular Assist Device (VAD) has Better Hemodynamic Effects on the Aorta than Constant Speed Mode: A Primary Numerical Study

Authors' Contribution:

Study Design A
Data Collection B
Statistical Analysis C
Data Interpretation D
Manuscript Preparation E
Literature Search F
Funds Collection G

BEF Kaiyun Gu
CDG Bin Gao
AG Yu Chang
A Yi Zeng

School of Life Sciences and BioEngineering, Beijing University of Technology, Beijing, P.R. China

Corresponding Author: Yu Chang, e-mail: changyu@bjut.edu.cn

Source of support: This work was partly sponsored by the National Natural Science Foundation of China (Grant No. 11272022, 11572014, 91430215). This work was also sponsored by Excellent Talents of Beijing (2013D008018000003, 2014000020124G045), and the Foundation (015000541115008, KM201510005028)

Background: BJUT-II VAD is a novel left ventricular assist device (LVADs), directly implanted into the ascending aorta. The pulsatile support mode is proposed to achieve better unloading performance than constant speed mode. However, the hemodynamic effects of this support mode on the aorta are still unclear. The aim of this study was to clarify the hemodynamic effects BJUT-II VAD under pulsatile support mode on the aorta.


Material/Methods: Computational fluid dynamics (CFD) studies, based on a patient-specific aortic geometric model, were conducted. Wall shear stress (WSS), averaged WSS (*avWSS*), oscillatory shear index (OSI), and averaged helicity density (Ha) were calculated to compare the differences in hemodynamic effects between pulsatile support mode and constant speed mode.

Results: The results show that *avWSS* under pulsatile support mode is significantly higher than that under constant speed mode (0.955Pa vs. 0.675Pa). Similarly, the OSI value under pulsatile mode is higher than that under constant speed mode (0.104 vs. 0.057). In addition, Ha under pulsatile mode for all selected cross-sections is larger than that under constant mode.

Conclusions: BJUT-II VAD, under pulsatile control mode, may prevent atherosclerosis lesions and aortic remodeling. The precise effects of pulsatile support mode on atherosclerosis and aortic remodeling need to be further studied in animal experiments.

MeSH Keywords: **Cardiovascular System • Heart-Assist Devices • Hemodynamics**

Full-text PDF: <http://www.medscimonit.com/abstract/index/idArt/896291>

 2736

 1

 10

 31



Background

Heart failure (HF) is a severe cardiovascular disease with high incidence and mortality rates. Left ventricular assist devices (LVADs) are widely used in heart failure treatment [1–4] to improve cardiac function recovery. The changes in cardiovascular hemodynamics caused by LVADs have been studied. For instance, Travis found that the blood pulsatility under LVADs support was significantly reduced [5]. Similarly, Tuzun reported that LVADs support could significantly increase the aortic impedance [6]. Ootaki demonstrated that the LVADs support may reduce coronary perfusion [7]. Callington reported that the flow pattern in the aortic root was significantly changed by LVAD support, which may be the reason for the abnormal of aortic valve function [8]. Cornwell demonstrated that the restoration of pulsatile flow through modulations in speed of LVAD led to increased distortion of the arterial baroreceptors with a subsequent decline in muscle sympathetic nerve activity, which was considered to benefit patient prognosis [9]. Ising reported that when the support level of LVAD is synchronous with the cardiac periods (named as the pulsatile support mode), the pulsatility of the blood flow was significantly enhanced [10]. The hemodynamic effects of LVADs under pulsatile support mode were studied, confirming that the pulsatile support mode could achieve better blood pulsatility and cardiac unloading performance [11–13].

BJUT-II VAD [14] is a novel LVAD, implanted into the ascending aorta (Figure 1). Its hemodynamic effects on the cardiovascular system have been studied. For instance, Xuan conducted computational fluid dynamic (CFD) simulation based on an idealized aortic model to evaluate the hemodynamic effect of BJUT-II VAD under constant speed mode on the aortic

flow pattern [15]. Subsequently, Gao compared the differences of hemodynamic effects of varied support modes (co-pulse mode, counter-pulse mode, and constant speed mode) on the cardiovascular system by utilizing a lumped parameters model and CFD method [16,17]. Zhang reported that the hemodynamic states of the coronary artery were significantly changed by BJUT-II VAD under varied support modes [18]. These studies demonstrated that the hemodynamic effects of BJUT-II VAD on the aorta are quite different from that caused by conventional LVADs, due to its special implanted position. The pulsatile support mode is a novel support mode, especially designed for BJUT-II VAD to improve the blood perfusion and left ventricular unloading level [19]. However, its hemodynamic effects on the aorta are still under investigation.

In this study, hemodynamic effects of the pulsatile support mode for the BJUT-II VAD on the aorta were studied by utilizing the CFD method. A patient-specific aortic model, based on CT data of a heart failure patient, was reconstructed. The hemodynamic effects generated by pulsatile support mode and constant speed mode were compared to clarify the different hemodynamic effects. Wall shear stress (WSS), averaged WSS ($avWSS$), oscillatory shear index (OSI), and averaged helicity density (H_d) were used as indicators to evaluate the hemodynamic states of the aorta under different support modes.

Material and Methods

Aortic model reconstruction

The aortic model was reconstructed by using MIMICS15.0 (MATERIALISE, BELGIUM) based on the CTA data from a heart

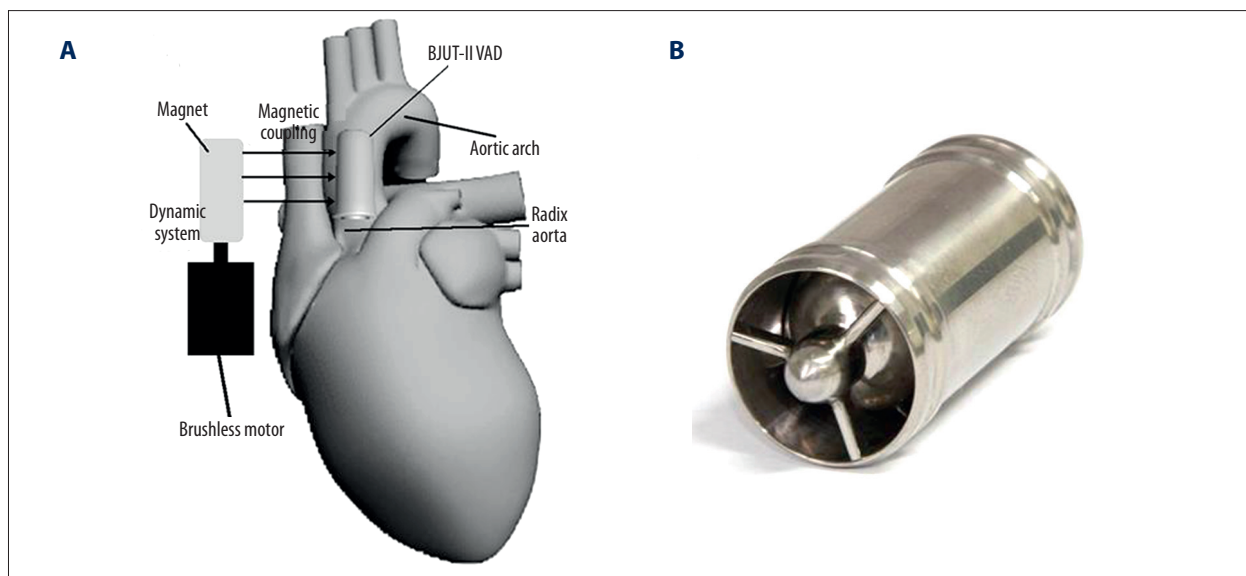


Figure 1. The scheme of BJUT-II VAD. (A) Shows the implanted position of BJUT-II VAD; (B) Presents the actual photos of BJUT-II VAD.

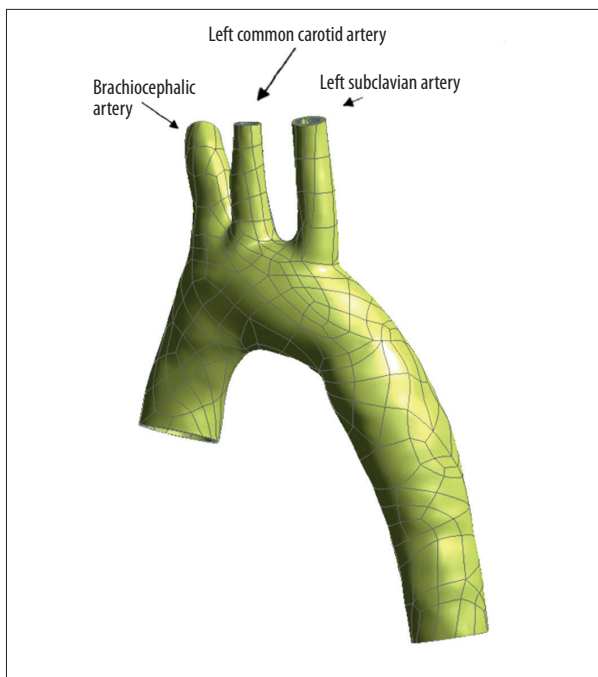


Figure 2. The reconstructed aortic model used in our work.

failure patient. The resolution of CTA data is 512 * 512, the pixel size is 0.91 mm, and the layer spacing is 1 mm. The aortic model (Figure 2) consisted of the ascending aorta, the brachiocephalic artery, the left common carotid artery, the left subclavian artery, and the descending aorta. The ANSYS ICEM 14.5 (ANSYS, Inc., USA) was used to generate the non-structural tetrahedral meshes for the model (Figure 3A, 3B). A grid independence test was conducted to determine the optimal grid numbers for the computation. In this test, the flow velocity was chosen as the inlet boundary condition, while free condition was imposed onto the outlets of the model as the boundary conditions. The relative errors of pressure at the inlet of the model with the different numbers of elements were calculated. If the relative error was less than 3%, the number of elements was considered to be sufficient. The test results are shown in Table 1. According to the results, 1,639,544 elements were sufficient for this study.

Numerical approaches

The blood flow is assumed as a 3D, incompressible, and laminar fluid. The blood flow is set as Newtonian and homogeneous with viscosity of 0.0035 P.s and density of 1.050 g/cm³. The deformation of the aortic wall was neglected. Gravitational force was assumed to be negligible. The governing equations are the continuity equations, as the equations (1) and (2):

$$\nabla \cdot v = 0 \tag{1}$$

$$\rho \frac{\partial v}{\partial t} + \rho(v \cdot \nabla)v = -\nabla p + \mu \nabla^2 v \tag{2}$$

where *v* is the blood flow velocity vector, *p* denotes pressure, ρ represents blood density, and μ is the dynamic viscosity. Aortic pressure was used as the boundary condition for the inlet, and velocities of blood flow were used as the boundary conditions for the outlets.

The boundary conditions for the study were derived from a validated lumped parameter model of assisted cardiovascular system (Figure 3C), which comprises left atria, active left ventricular, BJUT-II VAD, and peripheral circulation system. [18]. For the pulsatile support mode, the change in support level of BJUT-II VAD was synchronized with the cardiac period, while the support level under constant speed mode was constant during the whole cardiac period [16]. For both support modes, the time-dependent aortic pressure profiles (Figure 4) were used as the inlet boundary condition, and the blood flow was imposed onto the outlets of the model as the outlet boundary conditions (Figure 5A, 5B). In order to compare the hemodynamic effects of both support modes, the support level of both support modes were comparable, in which the mean arterial pressure was 85 mmHg and the mean blood flow was 5 L/min.

Computational settings

The commercial software FLUENT 14.5 (ANSYS, Inc., USA) was used for solving the set of fluid equations by using a finite-element scheme. The cardiac period was divided into 80 equally spaced time steps of 10 ms. Three cardiac periods were computed to obtain the result independent of initial conditions. Convergence was achieved when all mass, velocity component and energy changes, from iteration to iteration, were less than 10⁻⁶.

Hemodynamic analysis

Time-averaged wall shear stress (*avWSS*) [20], defined as the equation (3), was calculated to evaluate the distribution of WSS under both support modes:

$$avWSS = \frac{1}{T} \int_0^T |WSS_i| dt \tag{3}$$

where *WSS_i* represents the instantaneous wall shear stress at the *i*th node. *T* denotes the cardiac period and *t* is time.

The oscillatory shear index (OSI) [21] clarifies the WSS deviating from blood flow predominant direction during cardiac period, which is defined as the equation (4).

$$OSI = 0.5 \left\{ 1 - \frac{|\int_0^T WSS_i dt|}{\int_0^T |WSS_i| dt} \right\} \tag{4}$$

where the OSI value could vary from 0 to 0.5. 0 indicates no-cycle variation of WSS direction, while 0.5 indicates 180-degree deviation from WSS direction.

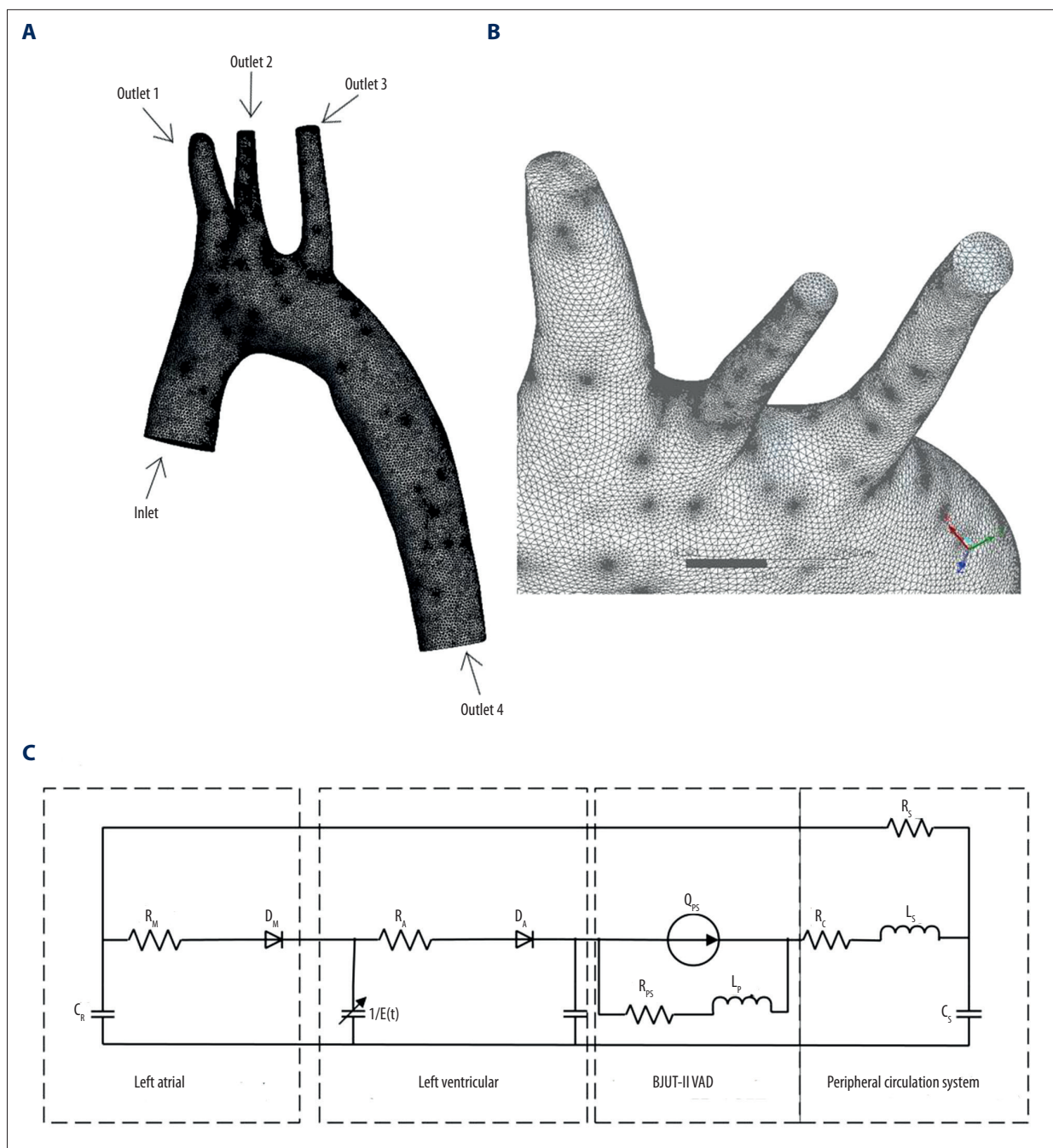


Figure 3. The aortic model with computational meshes. **(A)** Positions of inlet and outlets; **(B)** Partially enlarged view of the meshed model; **(C)** The cardiovascular pump system used to generate boundary condition for CFD study.

In order to characterize the change in strength of swirling flow in the aorta, the area-weighted averaged helicity density (H_a) [22] at several specific aortic cross-sections was defined as the equation (5):

$$H_a = \frac{1}{S} \int H_a dS \quad (5)$$

where S denotes the areas of the cross-sections. H_a represents the helicity density (the scalar product of velocity and vorticity in the flow field), defined as the equation (6):

$$H_a = v(\nabla \times v) \quad (6)$$

where v represents the blood flow velocity vector. $\nabla \times v$ is the vorticity of the blood flow.

Table 1. Results of analysis of grid independence.

Element size	Number of nodes	Number of elements	Reference value/kg*s ⁻¹	Error
1.2 mm	193216	1033661	5.296*10 ⁻²	
1 mm	298335	1639544	5.229*10 ⁻²	1.3%
0.7 mm	598556	3382639	5.217*10 ⁻²	0.2%

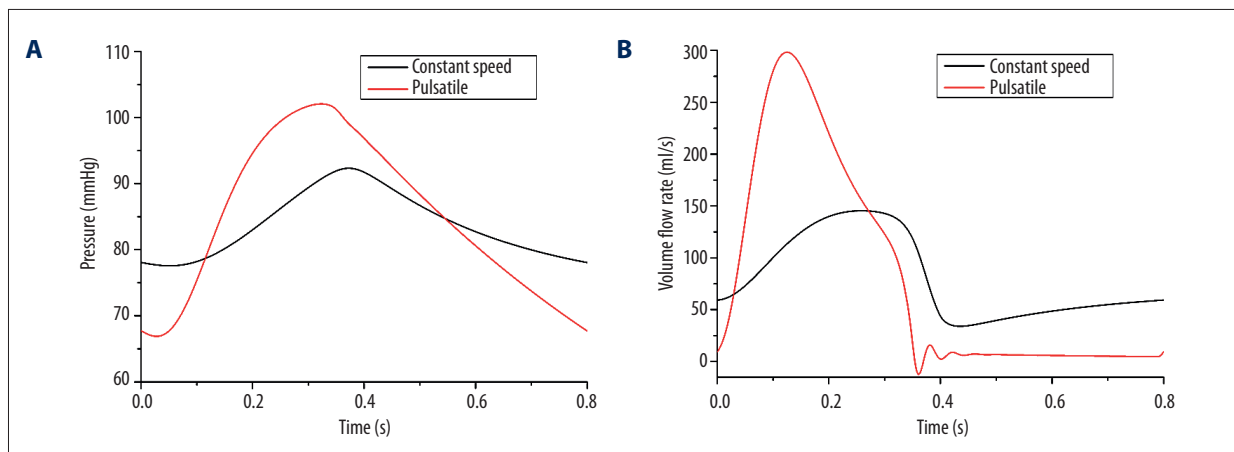


Figure 4. Boundary conditions of pressure and total volume flow rate. (A) The plot of pressure at the inlet of aorta under 2 support modes in 1 cardiac cycle. (B) The plot of volume flow rate under 2 support modes in 1 cardiac cycle.

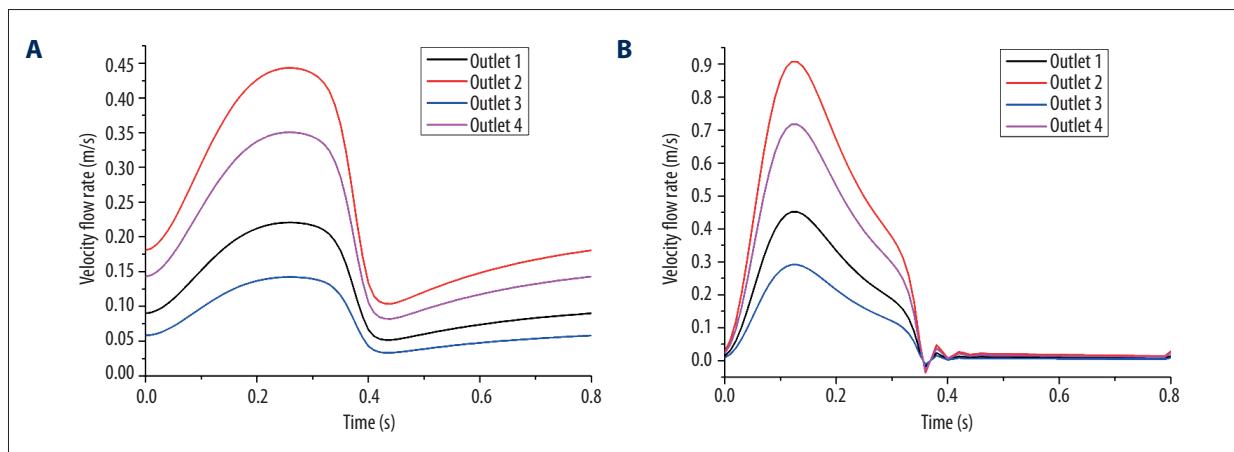


Figure 5. Boundary conditions of velocity flow rate for outlets. (A) The plot of velocity flow rate for outlets under constant speed mode in 1 cardiac cycle. (B) The plot of velocity flow rate for outlets under pulsatile mode in 1 cardiac cycle.

Results

In order to clearly illustrate the hemodynamic effects of varied support modes of BJUT-II VAD on the aorta, the distributions of *avWSS*, *OSI*, *H_a* were curved from Figures 6–10.

The distribution of *avWSS*

Figure 6 shows the distribution of *avWSS* in the aorta under both pulsatile support mode and constant speed mode. It is

seen that the distribution of *avWSS* under pulsatile support mode is similar with that under constant speed mode, while the value under the pulsatile support model is higher than that under constant speed mode (region a, b, and c). Under pulsatile support mode, *avWSS* ranged from 0.12 to 7.03Pa, while that under constant speed mode ranged from 0.05 to 6.95Pa. Under both modes, high *avWSS* were observed at the wall of the left common carotid artery, inner part of ascending aorta and aortic arch, and the posterior of the end of aortic arch;

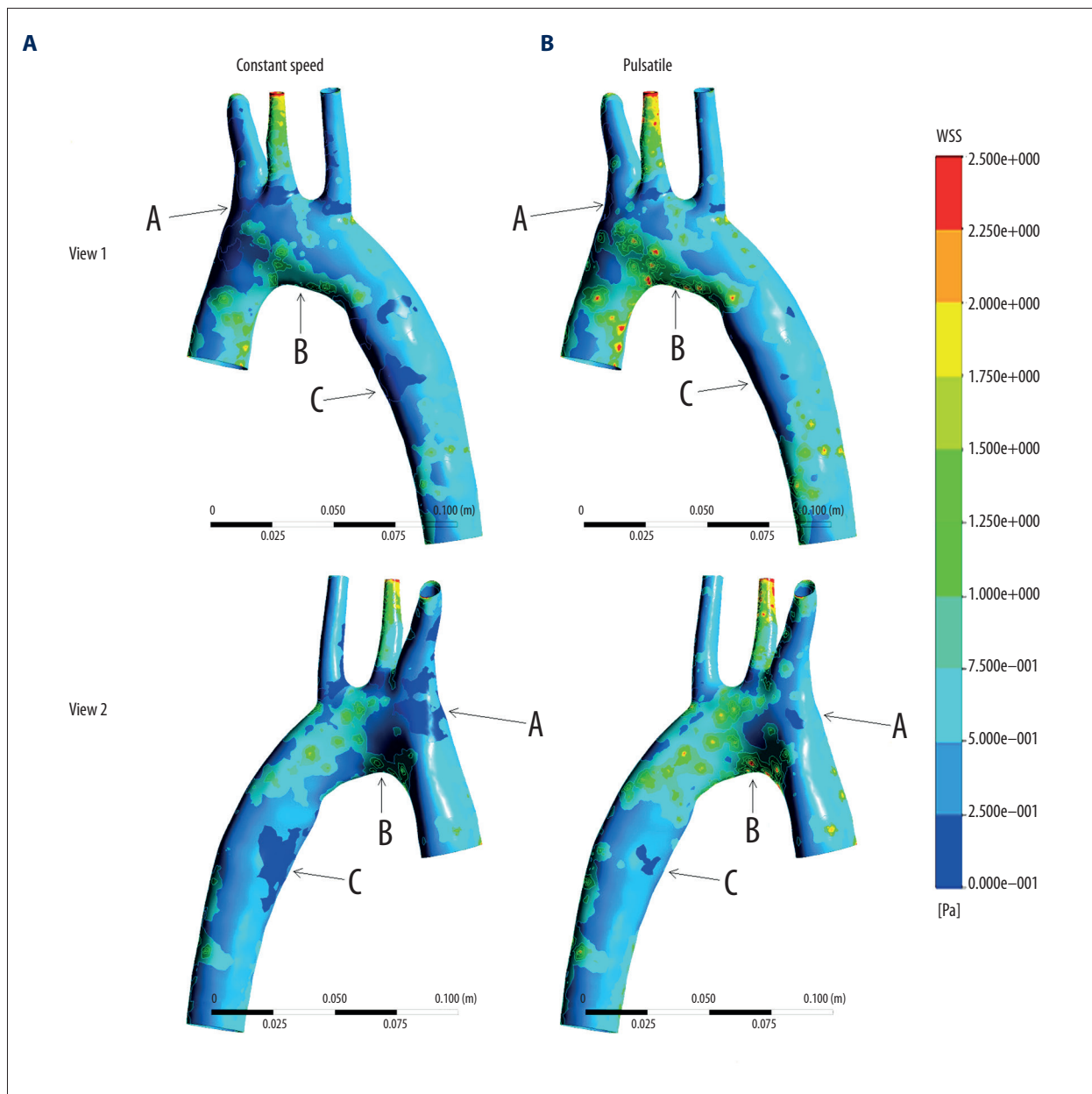


Figure 6. The distribution of time-averaged WSS under 2 support modes. (A) constant speed mode, (B) pulsatile mode.

while low *avWSS* regions are at the roots of the 3 branches and the inner of part of the descending aorta.

In order to more clearly illustrate the difference of *avWSS* under both support modes, the differences of *avWSS* at all nodes between the 2 modes are re-curved in Figure 7. In this figure, the value at each node is calculated by using the value under pulsatile support mode minus that under constant speed mode, showing that the *avWSS* under pulsatile mode are much higher than that under constant speed mode at the inner aortic arch and the 3 branch vessels (ranging from to 75% to 260%).

The distribution of OSI

The results of OSI for both constant speed mode and pulsatile mode are shown in Figure 8. The OSI under the constant speed mode ranged from 0 to 0.475, while that under pulsatile support mode ranged from 0 to 0.482. Although the range of OSI under both modes is similar with each other, the distribution is quite different. Under pulsatile mode, the OSI value at the descending aorta is significant higher than that under constant speed mode (Figure 8A, 8B).

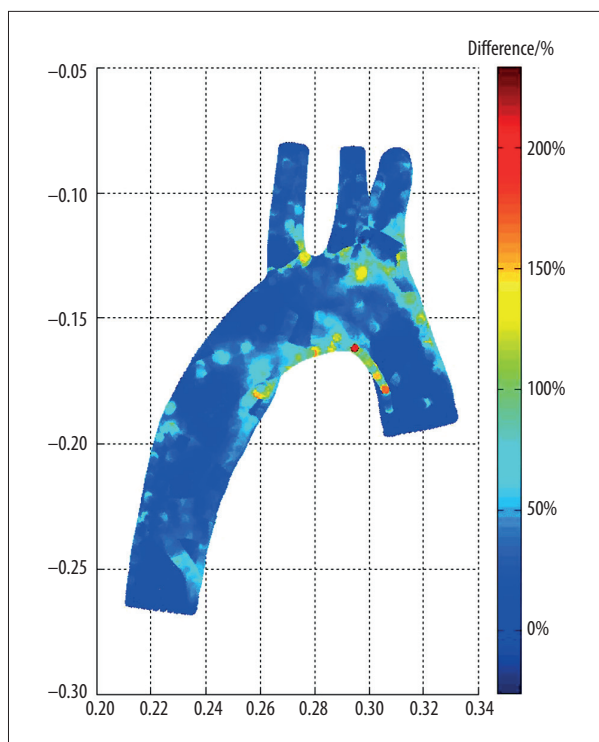


Figure 7. The difference of distribution of time-averaged WSS under 2 support modes.

The distribution of swirling flow

The swirling flow characteristics are shown in Figure 9 and Figure 10. Figure 9 illustrates the flow pattern of the swirling flow at 6 representative slices (from S1 to S6) along the aortic axial line (Figure 9A). Under both support modes, there was a detectable second flow at the walls of the ascending aorta. A small vortex is observed at the anterior wall of the ascending aorta (Figure 9B, 9C, S3). At the middle position of the aortic arch, the secondary flow was strengthened with 2 vortices formed along the anterior and the posterior walls (S4). When the blood flow moved into the posterior region of aortic arch, the vortex became stronger and the vortex, closing with the anterior aortic wall, became bigger, squeezing the posterior wall vortex into a narrow region, which exhibited clear characteristics of swirling flow (S5). And then, along with the flow entering into the descending aorta, the swirling flow formed at the aortic arch is gradually attenuated (S6). In order to evaluate the effect of varied support on the swirling flow, the H_a under both support modes was calculated (Figure 10). It is seen that under both modes, H_a achieved its maximum at the middle of the aortic arch, and then is attenuated along with the blood flow. In addition, under pulsatile flow mode, H_a at each slice is significantly higher than that under constant speed mode.

Discussion

The support mode of BJUT-II VAD is a very important factor in the hemodynamic effects on the cardiovascular system [16]. The pulsatile support mode of BJUT-II VAD, proposed by Gao et al. [19], is confirmed to be a better support mode for BJUT-II VAD. It has been proven that the pulsatile support mode can achieve better left ventricular unloading, higher arterial blood pulsatility, and better myocardial perfusion [23]. However, its effects on aortic hemodynamics are still under investigation. This study is the first study on the hemodynamic effects of pulsatile support mode on the aorta.

The link between hemodynamics and atherosclerosis and thrombosis has been studied for decades by clinicians and researchers [20,21,24]. There are studies indicating that low and reciprocating shear stress induce a sustained activation of atherogenic genes in endothelial cells (ECs) of vessel walls [25]. Wall shear stress (WSS) and oscillatory shear index (OSI) were reported as hemodynamic metrics that were associated with atherosclerosis localization and other aspects of vascular disease [26,27]. Hence, we used WSS and OSI to estimate the possible location of atherosclerosis lesions that may be generated under constant speed and pulsatile mode. The simulation results of $avWSS$ shown in Figure 6 shows that blood flow under pulsatile mode can cause higher WSS on the wall of the aorta than constant speed mode, which is determined by the velocity gradients between blood flow and the aorta wall. Although the total volume flow of blood under these 2 modes are similar in a cardiac cycle and the velocity of blood is in a positive correlation with the volume flow rate, the rapidly-changed volume flow rate of pulsatile mode may have a more significant effect on vessel walls. Comparing the 2 modes, the locations with low shear stress (Region A, C) and high shear stress (Region B) are distributed similarly, while the local specific values are significantly different. As shown in Figure 7, the value of $avWSS$ has a greater than 70% difference at the roots of branches of the brachiocephalic artery, left common carotid artery, and left subclavian artery, and the inner part of the aortic arch. This result reveals that, compared with the constant speed mode, the pulsatile support mode can achieve a relatively higher WSS and OSI distribution. Because these areas are preferential localization of atherosclerotic lesions, the increase of WSS under pulsatile mode may have an anti-atherogenic effect.

As shown in Figure 8, in most areas of the aorta under the constant speed, OSI is low, but in the area at roots of 3 branches (Region A), inner aortic arch (Region B), and upper-inner descending aorta (Region C), the OSI is relatively higher. For the whole aorta, OSI under the pulsatile mode has a similar distribution trend as the constant speed mode and higher value, which means that the pulsatile mode can generate more

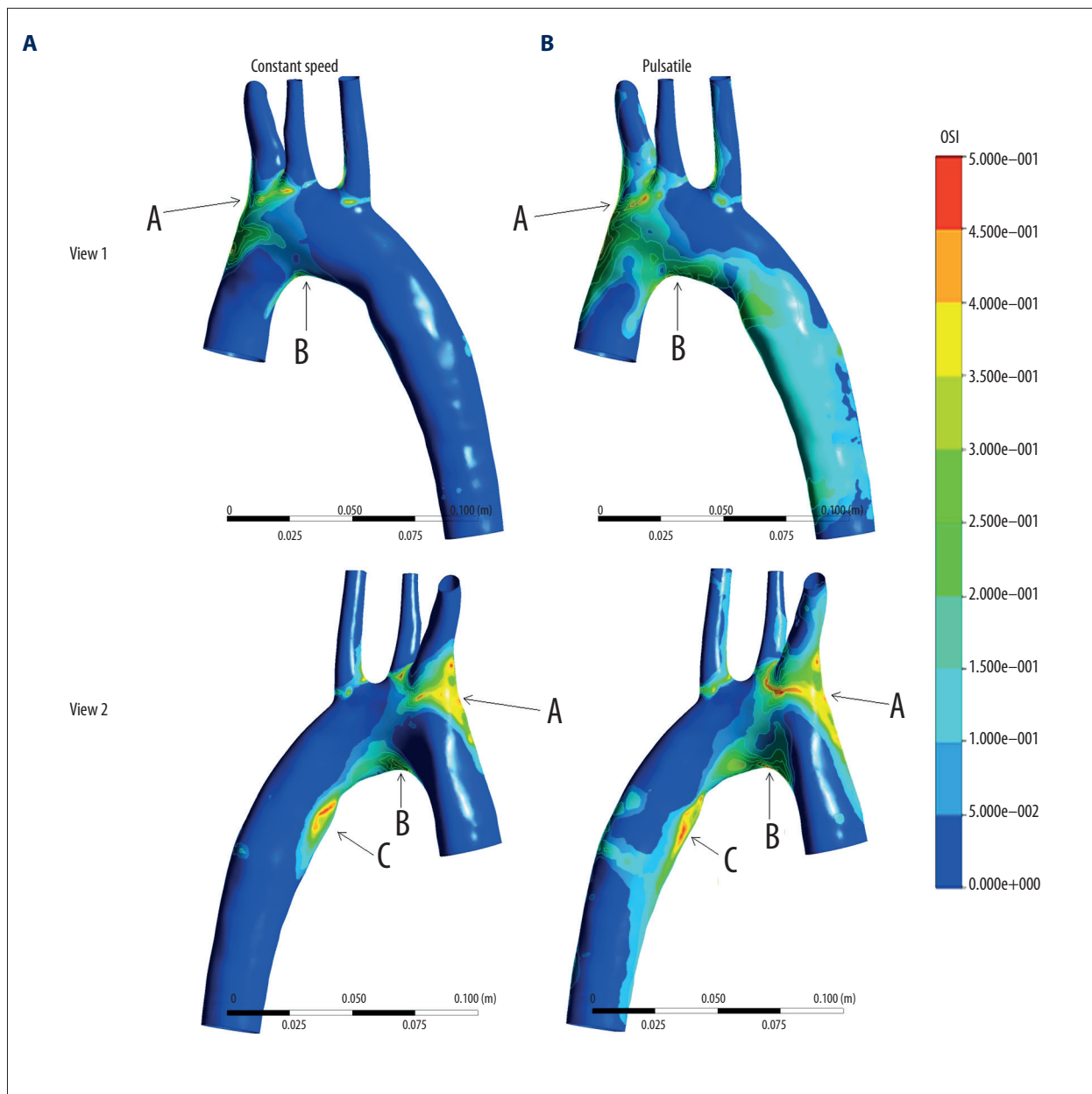


Figure 8. The distribution of OSI under 2 support modes. (A) Constant speed mode, (B) Pulsatile mode.

disturbed flow in a cardiac cycle. Combined with the results of OSI distribution and $avWSS$ distribution, the simulation shows that the areas with high OSI are usually located at the same areas as low $avWSS$ (Region A, C). This result is consistent with a simulation of blood mass transport of the aorta studied by Liu et al. [22]. Generally speaking, ring-like regions at the roots of each branch on the aorta arch and upper-inner descending aorta (Region A, C) with high OSI and low WSS have a high risk of generating atherosclerotic lesions.

Unlike the idealized model of the aorta used by Xuan et al. [15], the patient-specific model we used in the present study

has a more complicated geometric structure, especially curvatures at various directions, which can cause difficulty in identification and description of flow patterns in the aorta. Thus, the situation of helical flow was shown as a general description of averaged helicity density in this article. The complex geometry of the aorta induced helical flows at the curvature of the aortic arch [28,29], mainly occurring at the late phase of systole. It occupies a small part of the cardiac cycle, with a retrograde flow generated in the aortic arch at the end systole [28–30]. The volume flow rates (Figure 4B) are different in both the baseline and length of systole under different support modes we discussed, which caused obviously different

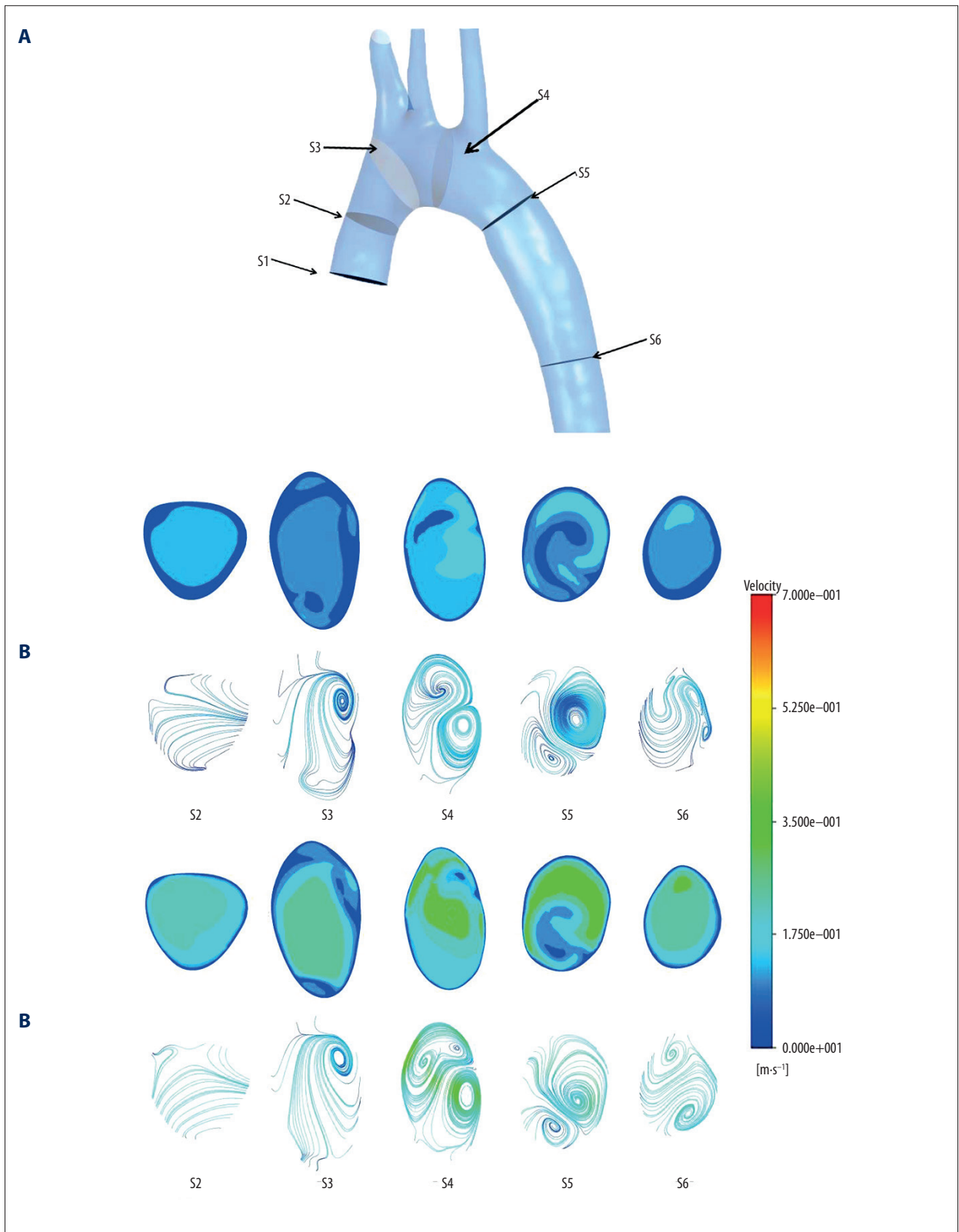


Figure 9. Results of helical flow distribution. **(A)** Positions of the representative slices for calculate H_a . **(B)** Contour and Streamline of velocity at the selected slices for constant speed mode. **(C)** Contour and Streamline of velocity at the selected slices for pulsatile mode.

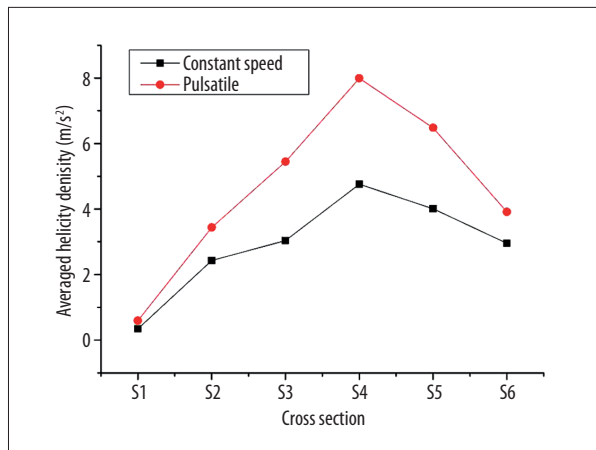


Figure 10. Plots of average of helicity density (H_d) at 6 representative slices.

occurrences of swirling flow (Figure 9). Liu et al. demonstrated the potential role of swirling flow in mass transport [22,31]. The helicity density enhanced under the pulsatile mode may have a positive effect in taking the deposited atherogenic lipids, such as low-density lipoproteins and particles, away from the luminal surface, which may spare the aorta from atherosclerosis, as well as improve the blood perfusion to organs [28,29].

Limitations of the study

To simplify the calculation, the aorta wall was assumed to be a rigid wall in the present study, without considering the effect

of elasticity of vessels. Investigations based on fluid-structure interaction should be undertaken to improve the precision of the simulation. Another limitation is that the aortic model was a patient-specific model, while the boundary conditions used in the simulation were idealized, and using only 1 patient-specific model is insufficient. Using patient-specific data from measurements as boundary conditions may make the simulation more realistic.

Conclusions

In comparison with the constant speed mode, the blood flow under pulsatile mode significantly enhanced WSS at the areas with relatively low WSS and high OSI under the constant speed mode. The higher helicity density of the blood flow under pulsatile mode may improve mass transport between the aortic luminal surface and blood flow. These findings indicate that pulsatile support mode is beneficial for reducing the risk of atherogenesis. However, the higher OSI of pulsatile support mode may also have negative effects on vascular remodeling. In short, the study results demonstrate that the BJUT-II VAD under pulsatile control mode may help prevent atherosclerosis lesions. The precise effects of pulsatile support mode on atherosclerosis and aortic remodeling need to be further studied in animal experiments.

References:

- Garbade J, Bittner HB, Barten MJ et al: Current trends in implantable left ventricular assist devices. *Cardiol Res Pract*, 2011; 2011: 290561-69
- Stevenson LW, Rose EA: Left ventricular assist devices: bridges to transplantation, recovery, and destination for whom? *Circulation*, 2003; 108(25): 3059-63
- Samak M, Fatullayev J, Sabashnikov A et al: Past and present of total artificial heart therapy: A success story. *Med Sci Monit Basic Res*, 2015; 21: 183-90
- Religa G, Jasińska M, Czyżewski L et al: The effect of the sequential therapy in end-stage heart failure (ESHF) – from ECMO, through the use of implantable pump for a pneumatic heart assist system, Religa Heart EXT, as a bridge for orthotopic heart transplant (OHT). Case study. *Ann Transplant*, 2014; 19: 537-40
- Travis AR, Giridharan GA, Pantalos GM et al: Vascular pulsatility in patients with a pulsatile- or continuous-flow ventricular assist device. *J Thorac Cardiovasc Surg*, 2007; 133(2): 517-24
- Tuzun E, Eya K, Chee HK et al: Myocardial hemodynamics, physiology, and perfusion with an axial flow left ventricular assist device in the calf. *ASAIO J*, 2004; 50(1): 47-53
- Ootaki Y, Kamohara K, Akiyama M et al: Phasic coronary blood flow pattern during a continuous flow left ventricular assist support. *Eur J Cardiothorac Surg*, 2005; 28(5): 711-16
- Callington A, Long Q, Mohite P et al: Computational fluid dynamic study of hemodynamic effects on aortic root blood flow of systematically varied left ventricular assist device graft anastomosis design. *J Thorac Cardiovasc Surg*, 2015; 150(3): 696-704
- Cornwell WK, Tarumi T, Stickford A et al: Restoration of pulsatile flow reduces sympathetic nerve activity among individuals with continuous-flow left ventricular assist devices. *Circulation*, 2015 [Epub ahead of print]
- Ising M, Warren S, Sobieski MA et al: Flow modulation algorithms for continuous flow left ventricular assist devices to increase vascular pulsatility: A computer simulation study. *Cardiovasc Eng Technol*, 2011; 2(2): 90-100
- Poullis M: Pulsatile mode of operation of left ventricular assist devices and pulmonary haemodynamics. *Interact Cardiovasc Thorac Surg*, 2014; 19(1): 11-15
- Karmonik C, Partovi S, Schmack B et al: Comparison of hemodynamics in the ascending aorta between pulsatile and continuous flow left ventricular assist devices using computational fluid dynamics based on computed tomography images. *Artif Organs*, 2014; 38(2): 142-48
- Bartoli CR, Giridharan GA, Litwak KN et al: Hemodynamic responses to continuous versus pulsatile mechanical unloading of the failing left ventricle. *ASAIO J*, 2010; 56(5): 410-16
- Chang Y, Gao B: Modeling and identification of an intra-aorta pump. *ASAIO J*, 2010; 56(6): 504-9
- Xuan Y, Chang Y, Gu K et al: Hemodynamic simulation study of a novel intra-aorta left ventricular assist device. *ASAIO J*, 2012; 58(5): 462-69
- Gao B, Chang Y, Xuan Y et al: The hemodynamic effect of the support mode for the intra-aorta pump on the cardiovascular system. *Artif Organs*, 2013; 37(2): 157-65
- Zhang Q, Gao B, Gu K et al: The study on hemodynamic effect of varied support models of BJUT-II VAD on coronary artery: A primary CFD study. *ASAIO J*, 2014; 60(6): 643-51

18. Gu K, Gao B, Chang Y et al: The hemodynamic effect of phase differences between the BJUT-II ventricular assist device and native heart on the cardiovascular system. *Artif Organs*, 2014; 38(11): 914–23
19. Gao B, Chang Y, Gu K et al: A pulsatile control algorithm of continuous-flow pump for heart recovery. *ASAIO J*, 2012; 58(4): 343–52
20. Ku DN: Blood flow in arteries. *Annu Rev Fluid Mech*, 1997; 29(1): 399–434
21. Ku DN, Giddens DP, Zarins CK et al: Pulsatile flow and atherosclerosis in the human carotid bifurcation. positive correlation between plaque location and low oscillating shear stress. *Arteriosclerosis*, 1985; 5(3): 293–302
22. Liu X, Fan Y, Deng X et al: Effect of non-Newtonian and pulsatile blood flow on mass transport in the human aorta. *J Biomech*, 2011; 44(6): 1123–31
23. Song Z, Gu K, Gao B et al: Hemodynamic effects of various support modes of continuous flow LVADs on the cardiovascular system: A numerical study. *Med Sci Monit*, 2014; 20: 733–41
24. Fatullayev J, Samak M, Sabashnikov A et al: Continuous-flow left ventricular assist device thrombosis: A danger foreseen is a danger avoided. *Med Sci Monit Basic Res*. 2015; 21: 141–44
25. Chiu JJ, Chien S: Effects of disturbed flow on vascular endothelium: pathophysiological basis and clinical perspectives. *Physiol Rev*, 2011; 91(1): 327–87
26. Steinman DA: Image-based computational fluid dynamics: A new paradigm for monitoring hemodynamics and atherosclerosis. *Curr Drug Targets Cardiovasc Haematol Disord*, 2004; 4(2): 183–97
27. Wootton DM, Ku DN: Fluid mechanics of vascular systems, diseases, and thrombosis. *Annu Rev Biomed Eng*, 1999; 1(1): 299–329
28. Kilner PJ, Yang GZ, Mohiaddin RH et al: Helical and retrograde secondary flow patterns in the aortic arch studied by three-directional magnetic resonance velocity mapping. *Circulation*, 1993; 88(5): 2235–47
29. Morbiducci U, Ponzini R, Rizzo G et al: *In vivo* quantification of helical blood flow in human aorta by time-resolved three-dimensional cine phase contrast magnetic resonance imaging. *Ann Biomed Eng*, 2009; 37(3): 516–31
30. Hope TA, Markl M, Wigström L et al: Comparison of flow patterns in ascending aortic aneurysms and volunteers using four-dimensional magnetic resonance velocity mapping. *J Magn Reson Imaging*, 2007; 26(6): 1471–79
31. Liu X, Pu F, Fan Y et al: A numerical study on the flow of blood and the transport of LDL in the human aorta: the physiological significance of the helical flow in the aortic arch. *Am J Physiol Heart Circ Physiol*, 2009; 297(1): 163–70